NASA Technical Memorandum 81759

NASA-TM-81759 19810016549

High-Response Measurements of a Turbofan Engine During Nonrecoverable Stall

Doug Lee
Lewis Research Center
Cleveland, Ohio

April 1981

NASA

HIGH-RESPONSE MEASUREMENTS OF A TURBOFAN ENGINE DURING NONRECOVERABLE STALL

by Doug Lee

National Aeronautics and Space Administration
Lewis Research Center
Cleveland, Ohio 44135

SUMMARY

This report presents high-response data recorded when a turbofan engine encountered nonrecoverable stall. High-response measurements of a Pratt and Whitney F100(3) turbofan engine at a simulated Mach number and altitude of 1.2 and 3000 m (10 000 ft) respectively were recorded during a nonrecoverable stall.

The nonrecoverable stall occurred as a result of incorrect scheduling of the high-compressor variable vanes (RCVV) during an experimental engine control investigation. Off-schedule RCVV was caused by a time lag in the RCVV switching mechanism during engine deceleration. Recorded data indicates rotating stall originating in the high-pressure compressor. From this region the disturbance propagates upstream into the fan and downstream throughout the core compressor.

Core compressor rotational speed had decreased, as a result of throttle movement, from 12 790 rpm to 10 800 rpm at the onset of stall. Rotating stall developed in the fan and high-pressure compressor at a frequency of 66 hertz. The rotating stall remained in the core compressor until the engine was shutdown. The fan exhibited some rotating stall, but the amplitude of the pressure oscillations were less severe. Data indicates that the fan was able to recover from the stall.

Fan turbine inlet temperature (FTIT) had been decreasing until stall developed in the high-pressure compressor. From this time, FTIT increased towards its maximum temperature limit. Increasing FTIT occurring with decreasing core compressor rotational speed is a trend exhibited by other F100 engines during nonrecoverable stall. The rising FTIT during nonrecoverable stall may be the result of incomplete combustion in the combustor and additional combustion occurring through the turbine.

E-822

INTRODUCTION

A nonrecoverable stall was observed in a Pratt and Whitney F100(3) turbofan engine during the evaluation of an experimental multivariable digital engine control system conducted at NASA-Lewis Research Center. Nonrecoverable stall is the inability of an engine compression system to recover from an engine stall, without engine shutdown to clear the stall. Although the research control played a part in the sequence of events leading to the stall, the research control was not the cause of the stall. The action which initiated the stall was the incorrect scheduling of the high-compressor variable vanes during transfer from research controls to engine BOM controls. A review of the multivariable control system may be found in reference 1.

As part of the full-scale multivariable control program, the engine could be controlled by the standard bill-of-material (BOM) control or the

research multivariable control (MVCS). Transfer from one control system to the other could be executed during engine operation. High-response as well as steady-state instrumentation were installed in the engine. Accordingly, outputs from these instruments were recorded on high-speed and steady-state devices. High-response measurements are presented. Data presented consist of plotted digital data and analog traces.

APPARATUS

A. Engine

The F100 engine, XD-11, used in this investigation is an F100(3) engine. The powerplant is a low-bypass, high-compression ratio, twin-spool turbofan with a mixed flow augmentor. A more complete description of the engine can be found in references 2 and 3. The basic F100 engine is controlled by a hydromechanical Unified Fuel Control (UFC) which provides primary and some secondary control functions. In addition to the UFC, a digital electronic engine control (EEC) provides trimming capability.

B. Multivariable Control System

The purpose of the multivariable research control program was to validate and demonstrate the applicability of linear quadratic regulator theory to the design of a propulsion control system (ref. 4). Five engine variables were controlled by the MVCS: Main burner fuel flow (WFMBH), exhaust nozzle thrust area (ANMIX), fan inlet guide vane angle (CIVV), compressor stator vane angle (RCVV) and compressor exit bleed flow (WBLC). The commands to control the electroservo system, which physically operated the control parameters, could be switched to originate from either the MVCS or bill-of-material (BOM) engine control at anytime.

C. Facility

The test program was conducted at NASA-Lewis's Propulsion System Laboratory 1 (PSL-1) altitude chamber. It is a conventional direct-connect engine installation (fig. 1). The chamber included a forward bulkhead, which separated the inlet plenum from the test chamber. Air of the desired temperature and pressure flowed from the plenum through the bellmouth to the inlet duct. Engine exhaust gases were captured by a collector which extended through the rear bulkhead, which minimized exhaust gas recirculation in the test chamber. A labyrinth seal is provided at the inlet duct-bulkhead interface to minimize static and dynamic interactions between engine and test facility.

D. Instrumentation

Instrumentation consisted of steady-state temperature and both steady-state and high-response pressures. Engine instrumentation designations are shown in figure 2. Detailed figures of steady-state and high-response instrumentation for each station also appear in figure 2.

Dynamic fan interstage (stations 2.1 to 2.3) and high-compressor interstage (stations 2.51 and 2.56) measurements consisted of outer wall static pressures only. Engine inlet (station 2.0), fan discharge (stations 2.5 and 2.5F), and compressor discharge (station 3.0) high-response measurements

included dynamic total pressure as well as some dynamic static pressures. No high-response temperature measurements were recorded.

High-response miniature pressure transducers were utilized. They were mounted in the rakes as close to the area of measurement as possible. To safeguard the physical integrity of the miniature transducers, water-cooling jackets were incorporated into the rake. An online calibration was performed prior to data recording in order to further minimize the effects of temperature and other factors on the transducer characteristics. Frequency response of the rake-transducer system was 500 hertz. Details of the high-response pressure-sensing rake can be found in reference 5.

E. Data Acquisition System

Steady-state pressures were acquired through a scanivalve system. Steady-state voltage levels of pressures and temperatures were gathered and digitized on a centralized recording system (ref. 6).

High-response data were acquired and recorded on two systems, Tradar and Central Analog. Tradar is a high-speed digital recording system with a maximum capacity of 200 channels. All 200 channels were used during this research program. The low-level voltage output of each probe was sequentially digitized and transmitted to a single recorder. The sampling rate of the high-speed digital recording system at the time of the stall was 4800 Hertz Thus, each of the 200 channels was sampled approximately every 42 milliseconds.

The second dynamic recording system utilized was Central Analog. This system is capable of recording 180 channels by FM multiplexing groups of 15 channels onto one of twelve available tracks using standard IRIG format. Recording tape speed was 120 inches per second. Playback speeds can be varied to provide different time scale expansions. The recorded analog samples are reproduced on a recording oscillograph.

RESULTS AND DISCUSSION

Data are presented for a sequence of events which precipitated the nonrecoverable stall. Table I outlines the sequence of events.

The engine was initially operating at intermediate throttle position on the research control system. A failure signal from the research system transferred operation of the engine to bill-of-material control. An automatic safety system retarded the throttle from intermediate to idle position immediately. The engine decelerated rapidly because of the throttle cutback. Momentary off-schedule operation of the RCVV's during the transfer concurrent with rapid engine deceleration was caused by excessive switchover time of the RCVV transfer valves. Off-schedule RCVV in the axial direction lowers the high-compressor stall line. The rapid deceleration and the lowered stall line resulted in high-compressor stall.

Recorded high-speed digital data are presented in figures 3 to 13. The solid symbol in these figures represent the last high-speed digital data point recorded just prior to the beginning of stall. The plotted data spanned the time from the start of throttle cutback to idle to engine shutdown.

The throttle (PLA) movement towards the idle position was initiated as a result of a safety action. PLA versus time is shown in figure 3. The throttle was at the idle position for approximately one second before stall originated. The engine was in stall for more than two and a half seconds

until the engine was shutdown. Core compressor speed (N2) versus time is plotted in figure 4. The plot shows core compressor speed continually decreasing from the time the throttle moved from intermediate to idle to off. High-compressor variable vane (RCVV) position versus time is seen in figure 5. The variable vanes are scheduled as a function of corrected compressor rotational speed. This is plotted in figure 6. The band between the two solid lines indicates the proper position of the vanes as a function of corrected compressor speed. Almost one and a half seconds elapsed between the times the vanes went off and back on schedule.

Engine inlet pressure (PT2), core compressor inlet pressure (PT25), fan duct inlet pressure (PT25F), core compressor exit pressure (PT3), burner pressure (PB) and fan turbine inlet temperature (FTIT) versus time are shown in figures 7 to 12, respectively. In these figures, the pressures and temperature are averages of individual measurements at various locations at that station. The location of the individual measurement may be found in the instrumentation schematic for that station in figure 2. No absolute conclusion may be drawn from the plots of the pressure data, since they are average measurements and the digitizer sampling rate is not adequate for exact stall analysis. These figures are presented to illustrate trends within the engine during this stall event. All the pressures except PB show a dramatic drop or rise in pressure level at the onset of stall. Again, with the exception of PB, the pressures oscillate after the initial surge. The oscillations indicate the presence of rotating stall.

Figure 12, the plot of FTIT versus time, shows that fan turbine inlet temperature decreases as the throttle was moved to the idle position. However, just after the appearance of stall in the engine compression system, the fan turbine inlet temperature rose towards its maximum temperature limit. FTIT continued to rise until approximately 2.8 seconds later when the engine was shutdown. FTIT began decreasing again when the engine was off. The plot of engine fuel flow (WFE) versus time, figure 13, reveals that fuel flow had decreased when the throttle was moved to idle and had remained at the idle flow until the engine was shut off. Whereupon, fuel flow dropped to zero. Decreasing high-compressor speed and increasing FTIT occurring simultaneously confirms the conclusion concerning F100 turbofan engine trends during nonrecoverable stall of reference 7.

In addition to the preceding plots, high-speed digital data were used to approximate core airflow and high-pressure turbine inlet temperature (T4). Core airflow was calculated based on an energy balance between the inlet of the core compressor and the exit of the high-pressure turbine. Two turbine inlet temperatures were calculated. The first, T4c, was based on an energy balance between the core compressor and high-pressure turbine. The second, T4n, is based on choked turbine nozzle flow. A detailed explanation of both methods of high-pressure turbine inlet temperature calculation is found in Appendix A. The temperatures calculated are provided as indications of the temperature trends at the high-pressure turbine inlet during the nonrecoverable stall. Since the calculations are based on steady-state measurements, no absolute quantitative results should be inferred.

The calculated combustor exit temperature based on an energy balance, T4c, is presented in figure 14. Combustor exit temperature based on choked turbine nozzle flow is seen in figure 15. The two methods of computing combustor exit temperature yield two different trends after the stall event. T4c based on energy balance increases after the stall, while T4n based on choked flow continues to decrease after the stall. Since T4c assumed complete burning of the fuel-air mixture in the combustor, T4c parallels the

trend seen in figure 13, FTIT versus time. Recorded measurements show FTIT increases after the stall and because T4n decreases after the stall, this suggests that complete combustion of the fuel-air mixture does not happen in the combustor but that some burning of the fuel-air mixture may continue through the high-pressure turbine.

The fan map, fan pressure ratio versus corrected fan airflow, is presented in figure 16. The steady-state stall and operating lines for the low-pressure compressor are outlined in figure 16 also. The fan comes down smoothly as the throttle is moved to idle. At the beginning of stall, the fan pressure ratio drops sharply. The fan pressure ratio oscillates while corrected fan airflow continues to decreaese. The pressure oscillations through the fan reduce in severity with time, indicating that the fan is recovering from the stall.

The compressor map, core pressure ratio versus corrected core airflow, is plotted in figure 17. Steady-state operating and stall lines are presented for reference. The progression of the high-pressure compressor into stall can be seen in this figure. The core compressor moves quickly from normal operation across the steady-state stall line. Core pressure ratio gradually decreases with decreasing corrected core airflow. At the onset of stall, core pressure ratio drops abruptly. The high-pressure compressor displays some oscillation after the stall and then cycles about a point on the compressor map. Greitzer, in reference 8, points out that a compression system, exhibiting the type of characteristics seen in figure 17, is in a rotating stall mode.

Another nonrecoverable stall occurred during a different full-scale engine research program conducted at NASA-Lewis Research Center. No high-response data suitable for stall analysis was available from this experimental augmentor program which also utilized a Pratt and Whitney F-100 engine. A periscope-mounted camera in the exhaust collector provided a view looking upstream into the engine. Photographs taken during the nonrecoverable stall encountered during the augmentor program can be seen in figures 18 to 20. In all three photographs, the large annular area with the bright spot in the lower right corner is the reflection of a spotlight on the external nozzle flaps. In the center of the annular area, the spoke pattern created by the swirl vanes mounted in the turbine exhaust case is well-defined. The bright rings seen between the spokes are the last stage of the low-pressure turbine. The first photograph, figure 18, shows the glow of the turbine during normal operation at intermediate throttle position. In the second photograph, figure 19, the augmentor had blown-out and the swirl of flame seen obscuring the right side flameholders is due to purging of the excess fuel remaining in the augmentor fuel manifold and lines. The ignition of which created a large pressure pulse to travel upstream in the fan duct, resulting in nonrecoverable stall in the engine. The third photograph, figure 20, was taken at intermediate throttle after the augmentor had blown-out and shutdown. Note the brighter glow in the last stage of the turbine as contrasted to what is seen in figure 18 for the same throttle position. This brighter glow in the turbine may possibly be attributed to the higher temperatures appearing in the turbine as combustion occurs through the turbine during nonrecoverable stall. Shutdown of the engine was required to remove the stall.

Analog traces of recorded high-response pressure measurements of the nonrecoverable stall caused by off-schedule RCVV are presented in figures 21 to 27. The initial surge cycle(s), followed by rotating stall, can clearly be seen in most of these traces. From these analog traces, the frequency of

rotating stall was determined to be 66 hertz. Reference 7 mentions rotating stall at a frequency of 65 hertz from analysis of their nonrecoverable stall. The chronological order that each pressure measurement saw the first sign of a significant pressure perturbation was determined from the analog traces and presented in table II. Pressure fluctuations at the fan discharge (stations 2.5 and 2.5F) and through the high-pressure compressor (stations 2.51 to 3.0) appear to be more severe and sustained than those in the low-pressure compressor (stations 2.0 to 2.3). Pressure fluctuations in the fan tend to decrease in amplitude with time. Generally, the pressure oscillations in the fan die out within half-a-second of the beginning of stall. The fan appears to be able to recover from the stall. At the fan discharge and in the high-pressure compressor, rotating stall is clearly defined. At these locations, the pressure fluctuations continued without diminishing amplitude until the engine was shutdown. The high-pressure compressor could not recover from the stall.

SUMMARY OF RESULTS

Nonrecoverable stall ocurred on an F-100(3) turbofan engine. High-response measurements were recorded and analyzed. Analysis determined:

1. Complete burning of the fuel-air mixture may not have occurred in the combustor and combustion of the remaining unburned mixture appears to have continued through the turbine.
2. Rear compressor variable vanes (RCVV) were not on-schedule during the power lever angle (PLA) excursion.
3. Off-schedule rear compressor variable vane (RCVV) lowered the high-pressure compressor stall line and brought the engine from the operating line through the stall line.
4. Stall originated in the core compressor.
5. After the initial surge, rotating stall developed with a frequency of 66 hertz in both the fan and core compressor.
6. Rotating stall was more severe and sustained in the high-pressure compressor while the fan seemed to recover.
7. Fan turbine inlet temperature (FTIT) increased after the stall developed.
8. Before FTIT reached its maximum temperature limit, the engine was shutdown as a safety precaution.

APPENDIX A - ESTIMATED HIGH TURBINE INLET TEMPERATURES

High-pressure turbine inlet temperatures were estimated by two methods. The first method was based on an energy balance across the combustor. The second method was based on choked turbine nozzle flow. Only steady-state thermocouple measurements were available for use in both methods.

Both methods required fuel-air ratio, f, as an input. Fuel-air ratio was determined by establishing an energy balance between the high-pressure compressor inlet (station 2.5) and the high-pressure turbine exit (station 4.5),

$$hg_{4.5}(1 + f) - ha_{2.5} = \eta(f)(LHV).$$

It was assumed that complete combustion of the fuel occurred between these two locations. Thus, combustion efficiency, η, is one hundred percent.

METHOD 1

This high turbine inlet temperature, T4c, is a function of the high-pressure compressor exit temperature plus the temperature rise due to combustion of fuel in the combustor and is approximated by,

$$T4c(1 + f) = T3 + \frac{\eta_c(f)(LHV)}{C_p}$$

For this method, complete combustion of all the fuel occurs in the combustor. Combustor efficiency, η_c, is one hundred percent.

METHOD 2

This high turbine inlet temperature, T4n, is based on choked turbine nozzle flow,

$$T4n = \frac{(FP_4)(P_B)}{Wg_4}^2 .$$

The flow parameter at this engine location, FP4, is determined from experimental data recorded prior to the nonrecoverable stall. P_B, the main burner pressure is a measured quantity. The total gas flow, W_{g4}, is the sum of the measured fuel flow (W_{fe}) and airflow at the high-pressure turbine inlet (W_{a4}). HPT inlet airflow can be derived from the fuel-air ratio calculated earlier.

APPENDIX B - SYMBOLS

C_p	coefficient of specific heat at constant pressure
f	fuel-air ratio in main combustor
FP4	flow parameter based on measured conditions at HPT inlet
HPC	high pressure compressor
HPT	high pressure turbine
$ha_{2.5}$	enthalpy of air based on HPC inlet temperature
$hg_{4.5}$	enthalpy of gas based on HPT exit temperature
LHV	lower heating value of fuel
η_c	combustor efficiency
P_B	main burner pressure
T3	HPC exit temperature
T4c	calculated HPT inlet temperature - METHOD 1
T4n	calculated HPT inlet temperature - METHOD 2
Wa4	airflow at HPT inlet
Wg4	total gas flow at HPT inlet
Wac	calculated HPC airflow
Wfe	measured main burner fuel flow

REFERENCES

1. Lehtinen B.; and Soeder, J. F.: The F100 Multivariable Control Synthesis Program: A Review of Full-Scale Engine Altitude Tests. Propulsion Controls, 1979. NASA CP-2137, 1980, pp. 20-34.

2. Sams, H.: F-15 Propulsion System Design and Development. AIAA Paper 75-1042, Aug. 1975.

3. Staley, E. I.: F-15 Propulsion Flight Testing Experience. AIAA Paper 75-1052, Aug. 1975.

4. Lehtinin B.; DeHoff, R. L.; and Hackney, R. D.: Multivariable Control Altitude Demonstration on the F100 Turbofan Engine. NASA TM-79183, 1979.

5. Armentrout, E. C.: Development of a High-Frequency Response Pressure-Sensing Rake for Turbofan Egine Tests. NASA TM X-1959, 1970.

6. Miller, R. L.: ESCORT: A Data Acquisition and Display System to Support Research Testing. NASA TM-78909, 1978.

7. Diaz, R.; Kelly, J. B.; and Thompson, F. B.: Data Base for Nonrecoverable Stall Investigation. PWA-FR-1212, Pratt & Whitney Aircraft Group, 1979 (AFAPL TR-79-2091, AD-B043393L.)

8. Greitzer, E. M.: Surge and Rotating Stall in Axial Flow Compressors, I - Theoretical Compression System Model. ASME Paper 75-GT-9, Mar. 1975.

TABLE I. - SEQUENCE OF EVENTS

Time				Event
Hr	Min	Sec	Msec	
03,	51,	33,	841	Transfer from research to BOM control
				Throttle trip to idle
				RCVV switching delay during transfer
				RCVV switching delay sets RCVV off-schedule (off-schedule RCVV in axial direction decreases high-pressure compressor stall margin)
03,	51,	34,	215	Throttle at idle
03,	51,	35,	135	Stall initiated
03,	51,	35,	214	FTIT increased
03,	51,	35,	755	RCVV on-schedule
03,	51	37,	876	engine shutdown

TABLE II. - CHRONOLOGICAL ORDER MEASUREMENTS FIRST SENSED DISTURBANCE

Msec, from 3:51:35.000	Parameter
134.8	pt 25 - 113 - 2 pt 25 - 293 - 3
135.7	pt 25f - 68 - 1 pt 25f - 248 - 2
136.7	pt 25 - 23 - 1 pt 252 - 43 - 0
137.7	ps 253 - 303 - 0
139.6	ps 23 - 258 - 0
141.6	ps 25f - 338 - 3
143.6	ps 254 - 292 - 0 pt 255 - 303 - 0
144.5	ps 251 - 312 - 0 ps 22 - 244 - 0
148.4	ps 22 - 64 - 0
157.0	ps 21 - 66 - 0
159.2	pt 3 - 67 - 1 pt 3 - 67 - 2
162.1	pt 3 - 292 - 1 pt 2 - 270 - 2
163.1	pt 3 - 292 - 2 ps 2 - 95 - 0 ps 2 - 275 - 0
164.1	pt 2 - 270 - 4
165.0	pt 2 - 90 - 2 pt 2 - 90 - 4

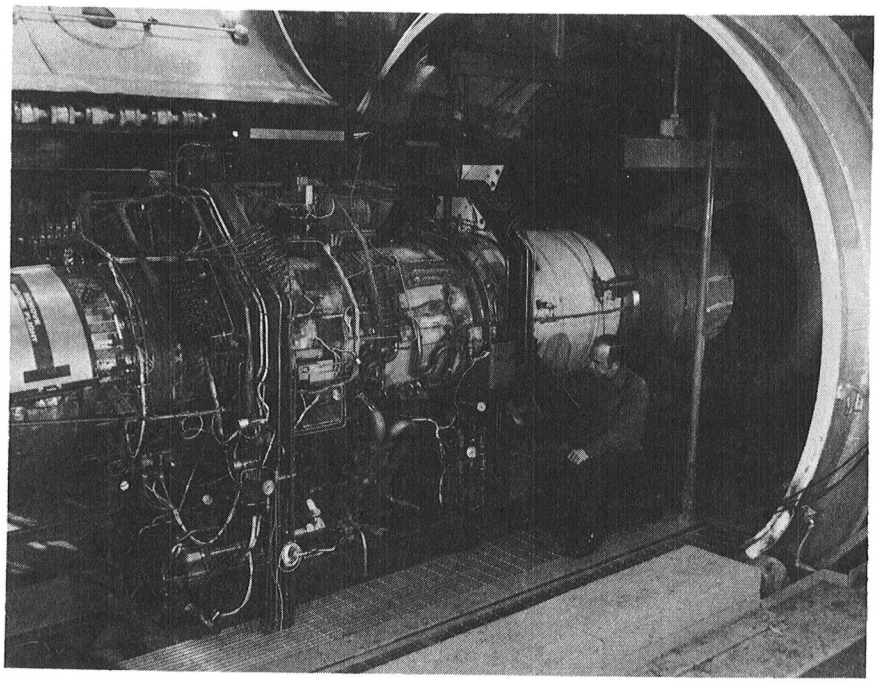

Figure 1. - F100(3)-XD11 Engine installation in altitude chamber.

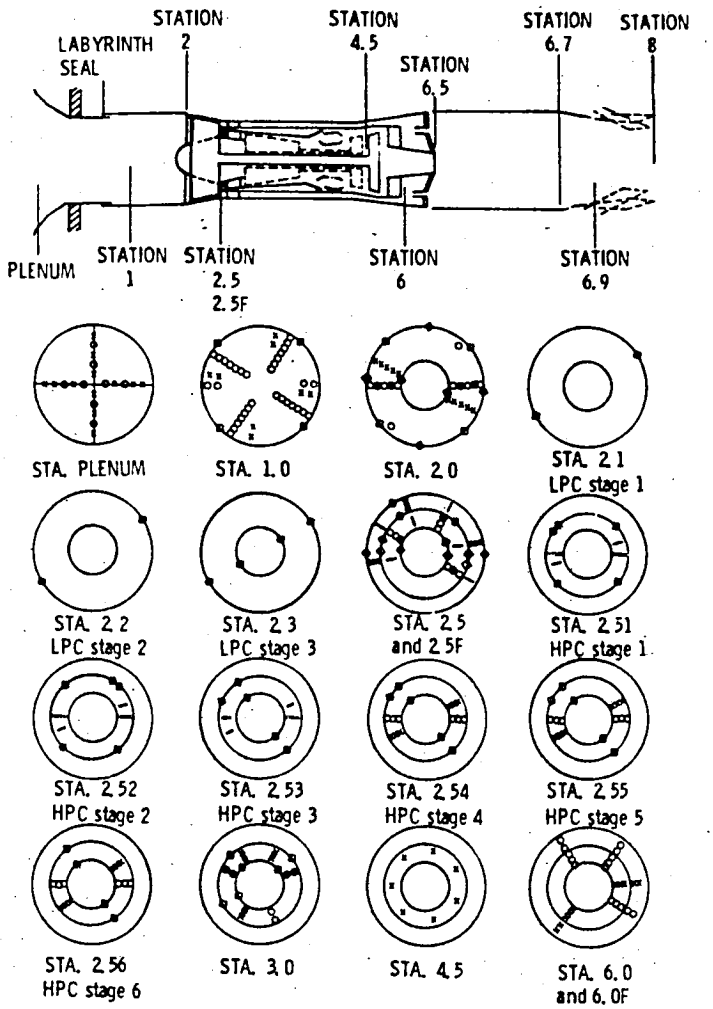

Figure 2. - Engine station designations and instrumentation locations.

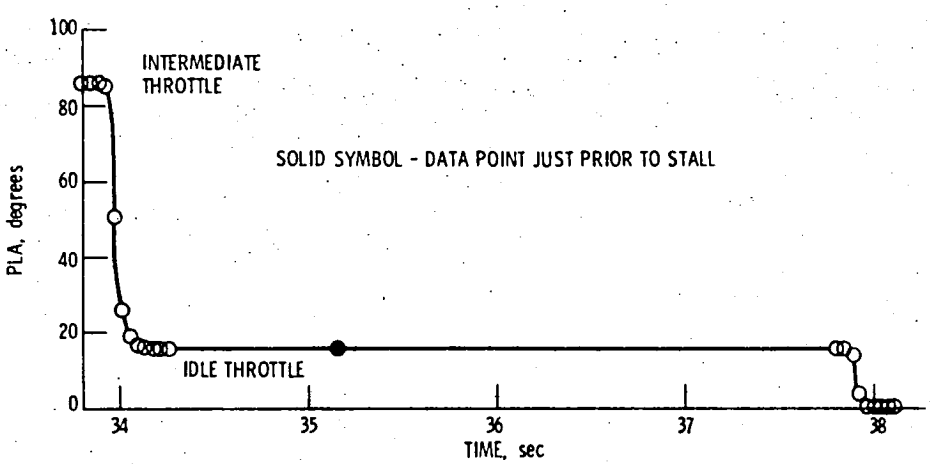

Figure 3. - Time history of power lever angle during the non-recoverable stall transient.

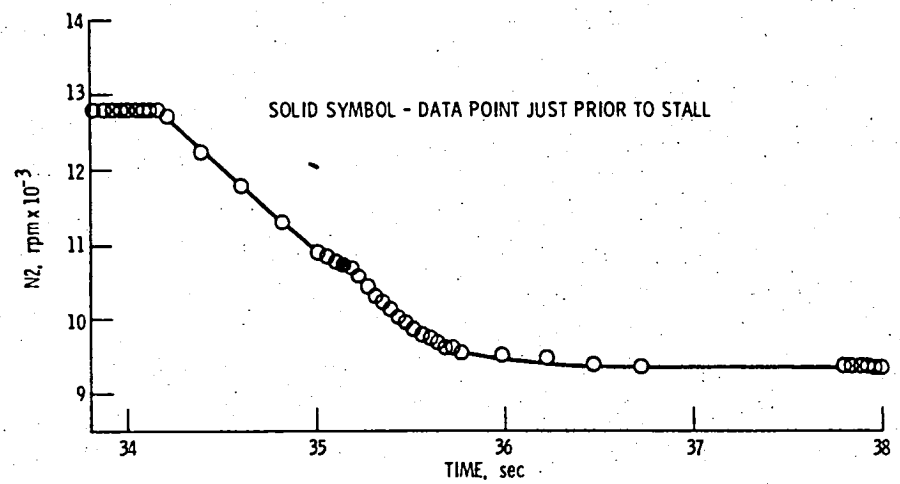

Figure 4. - Time history of high-compressor rotor speed during the non-recoverable stall transient.

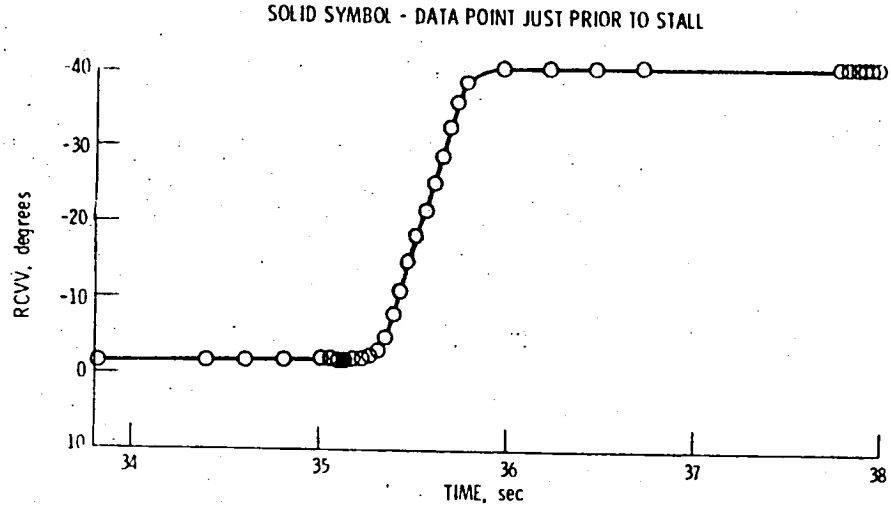

Figure 5. - Time history of rear compressor variable vanes during the non-recoverable stall transient.

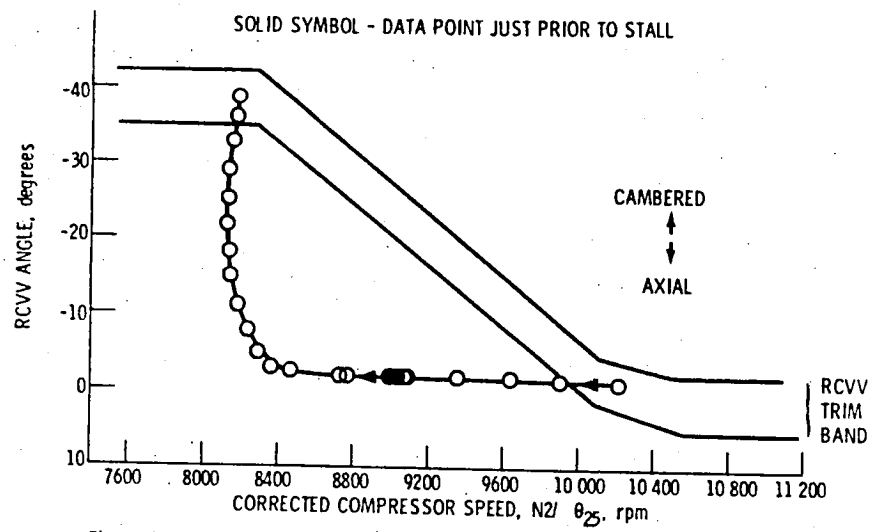

Figure 6. - Rear compressor variable vane excursion during the non-recoverable stall transient as a function corrected core compressor speed.

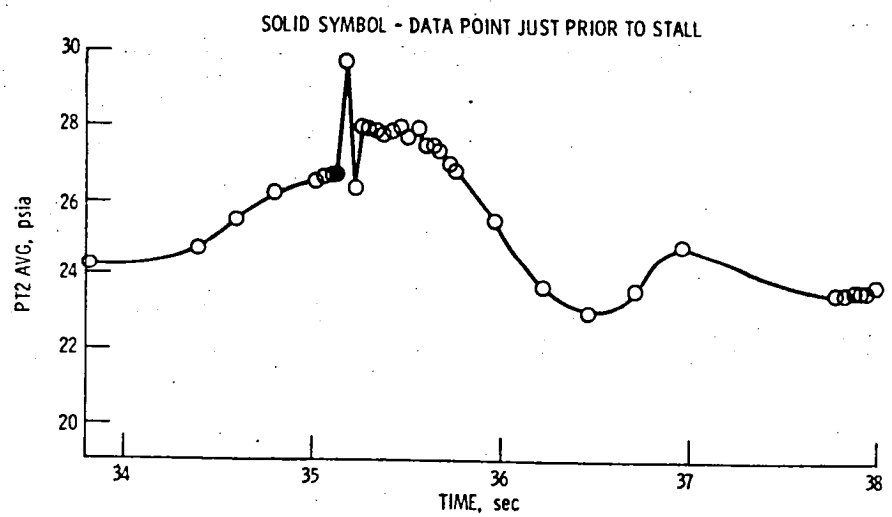

Figure 7. - Time history of average pressure at engine inlet during the non-recoverable stall transient.

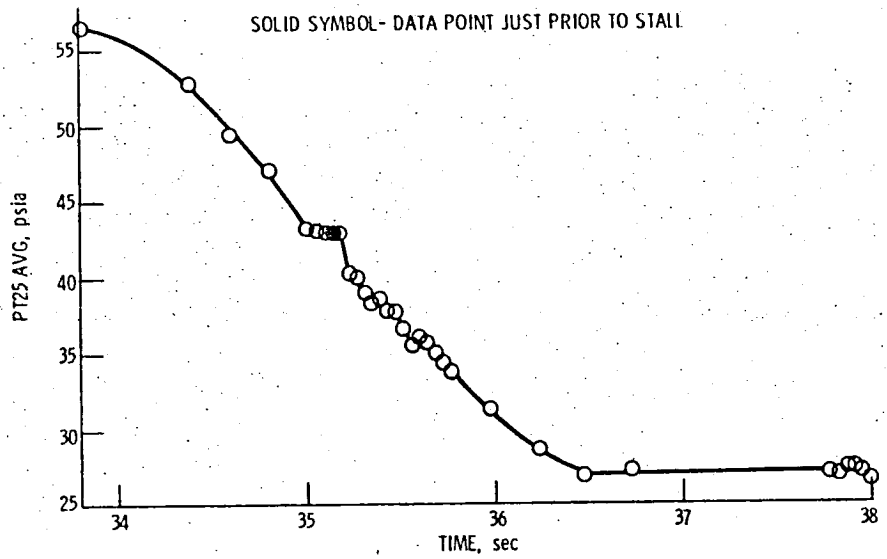

Figure 8. - Time history of average pressure at core compressor inlet during the non-recoverable stall transient.

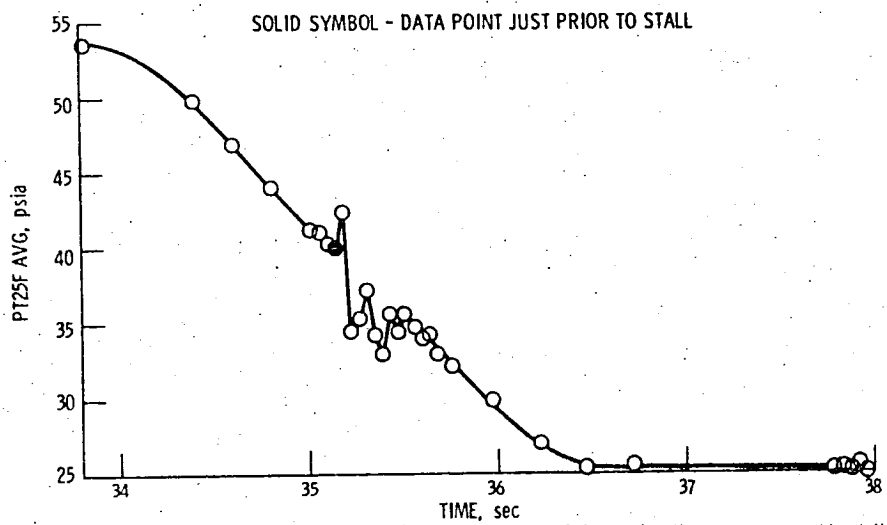

Figure 9. - Time history of average pressure at fan duct inlet during the non-recoverable stall transient.

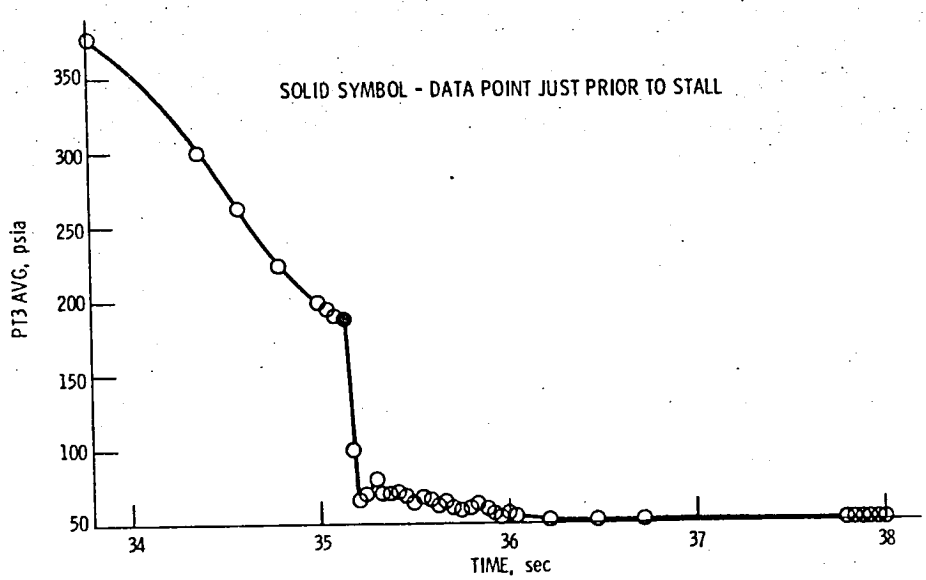

Figure 10. - Time history of average pressure at core compressor exit during the non-recoverable stall transient.

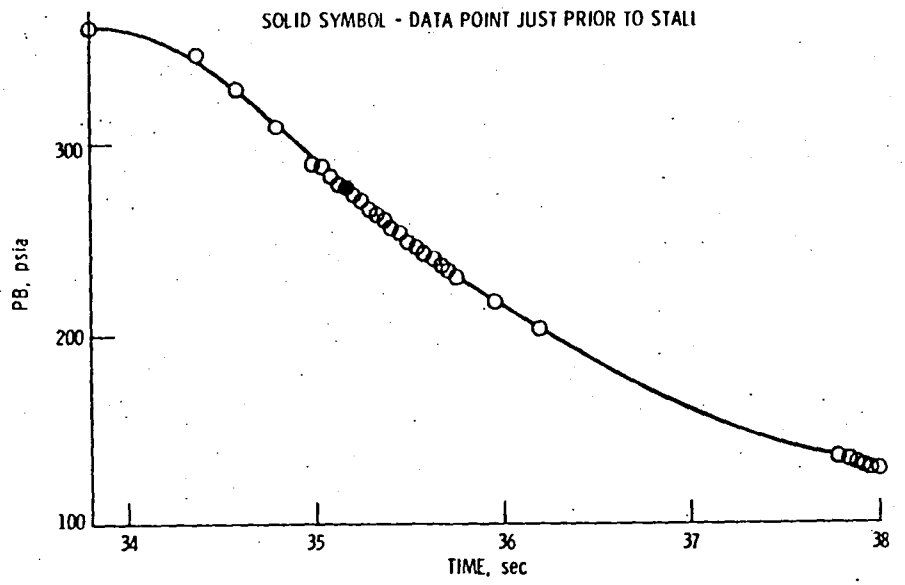

Figure 11. - Time history of burner pressure during the non-recoverable stall transient.

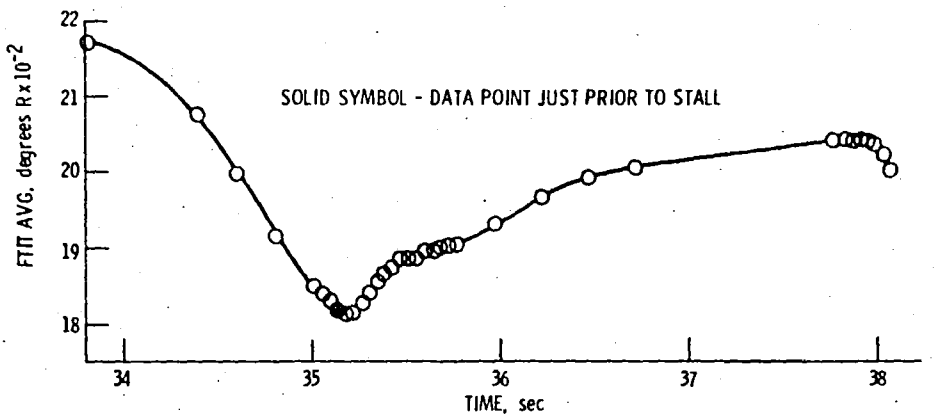

Figure 12. - Time history of average for turbine inlet temperature during the non-recoverable stall transient.

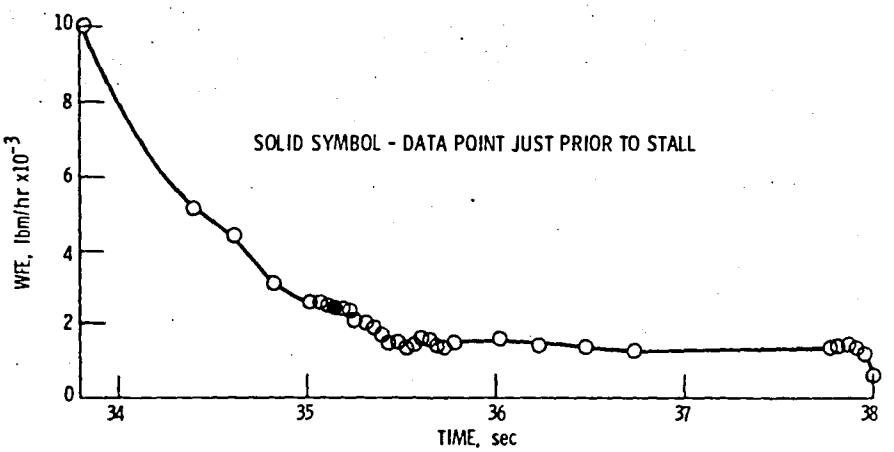

Figure 13. - Time history of engine fuel flow during the non-recoverable stall transient.

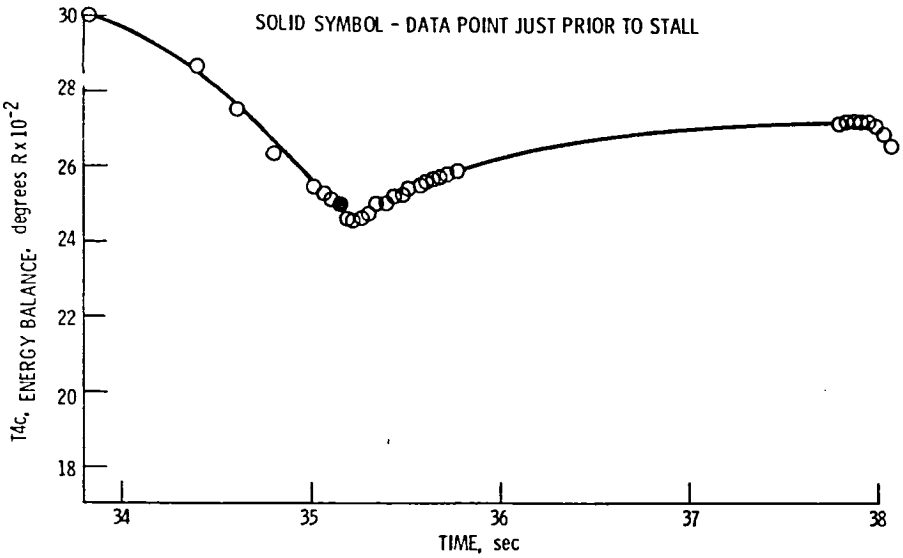

Figure 14. - Time history of calculated combustor exit temperature using energy balance during the non-recoverable stall transient.

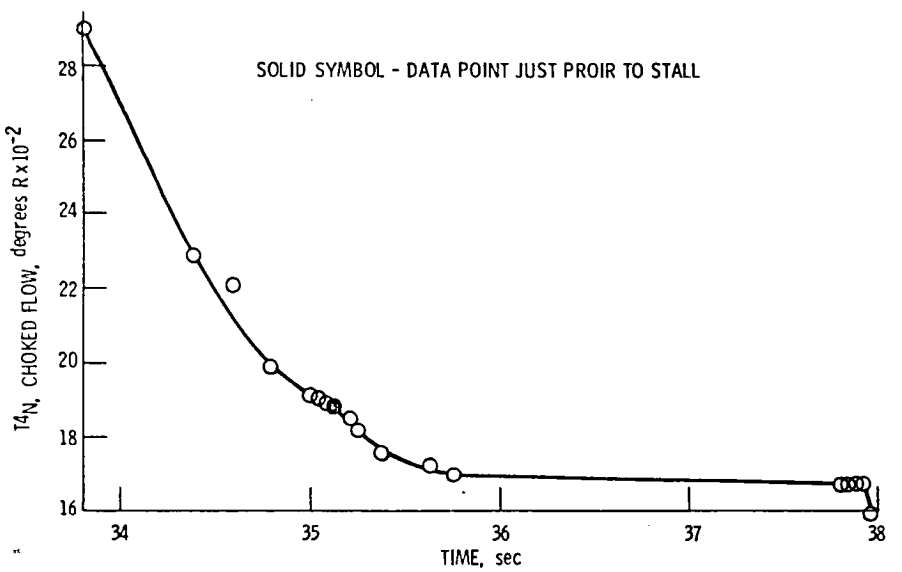

Figure 15. - Time history of computed combustor exit temperature based on choked turbine during the non-recoverable stall transient.

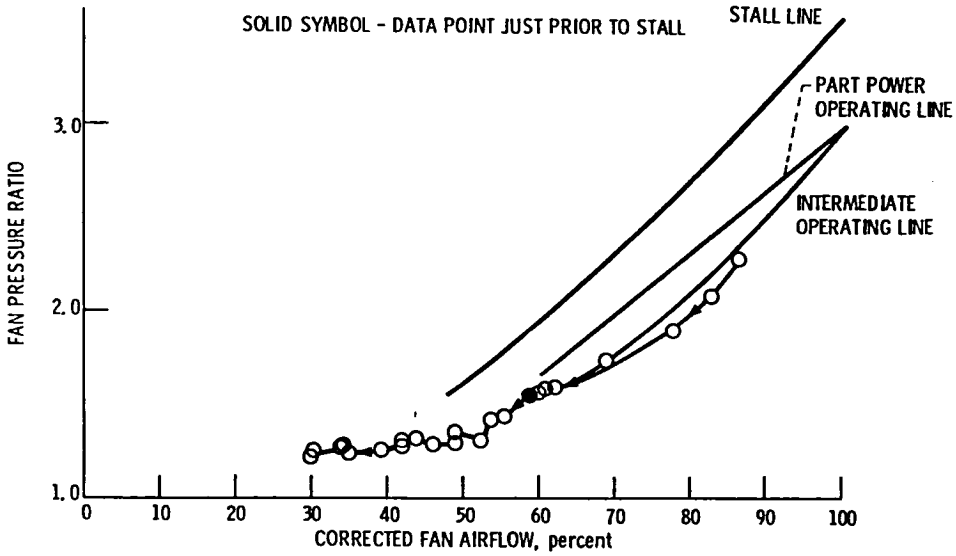

Figure 16. - Fan pressure ratio as a function of percent corrected fan airflow during the non-recoverable stall transient.

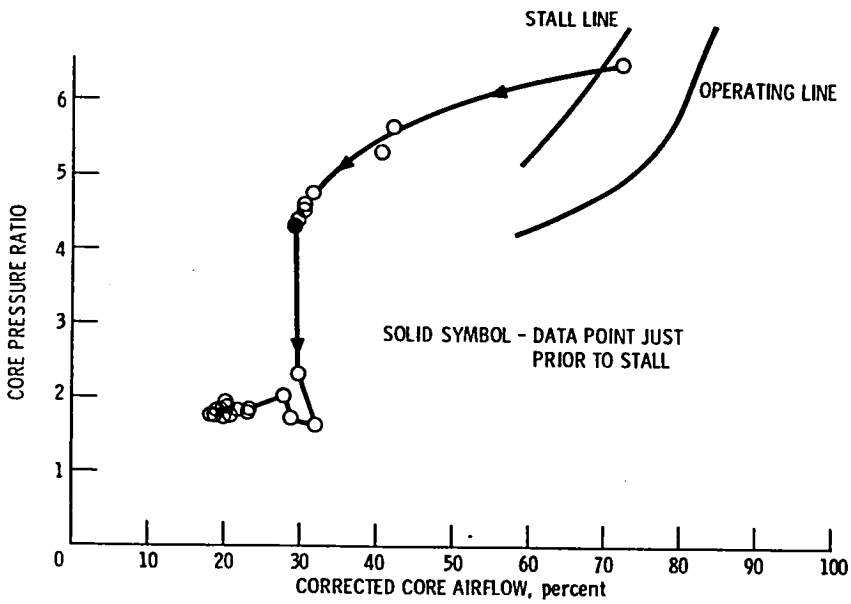

Figure 17. - Core compressor pressure ratio as a function of percent corrected core compressor airflow during the non-recoverable stall transient.

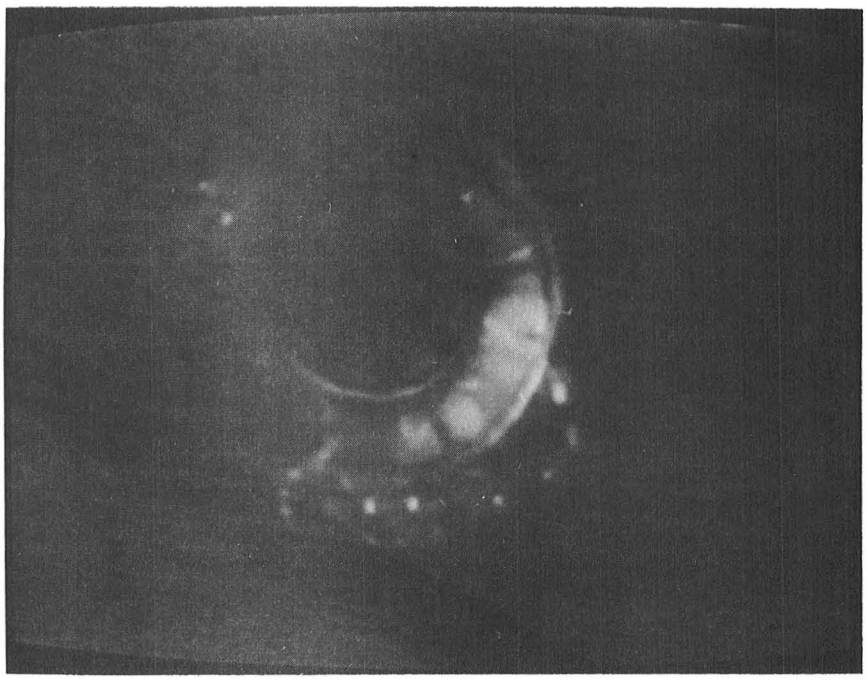

Figure 18. - Upstream view of engine during normal engine operation at intermediate throttle position.

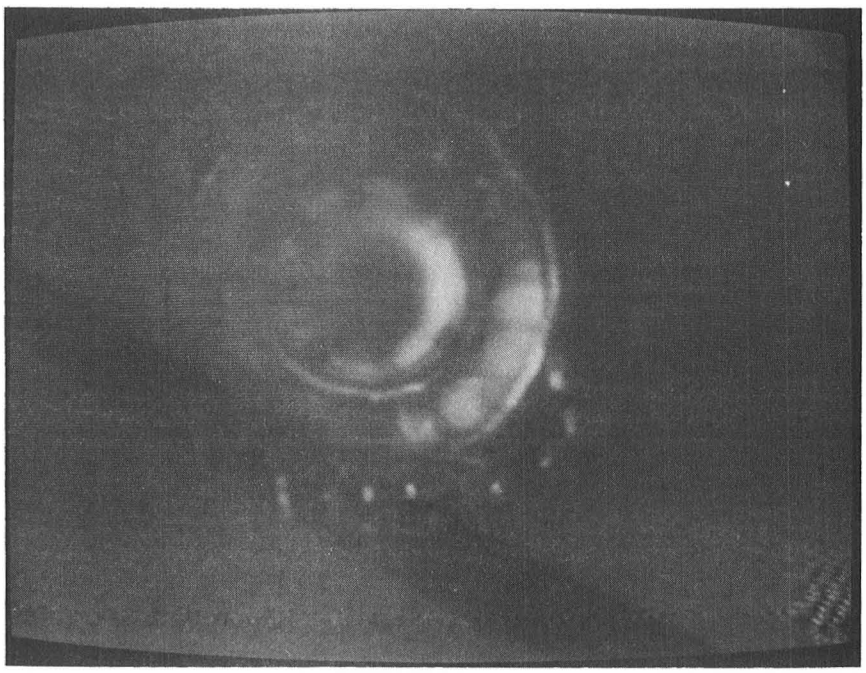

Figure 19. - Upstream view of engine after the augmentor had blown-out. Swirl of flame is due to combustion of the fuel from purging the augmentor fuel lines.

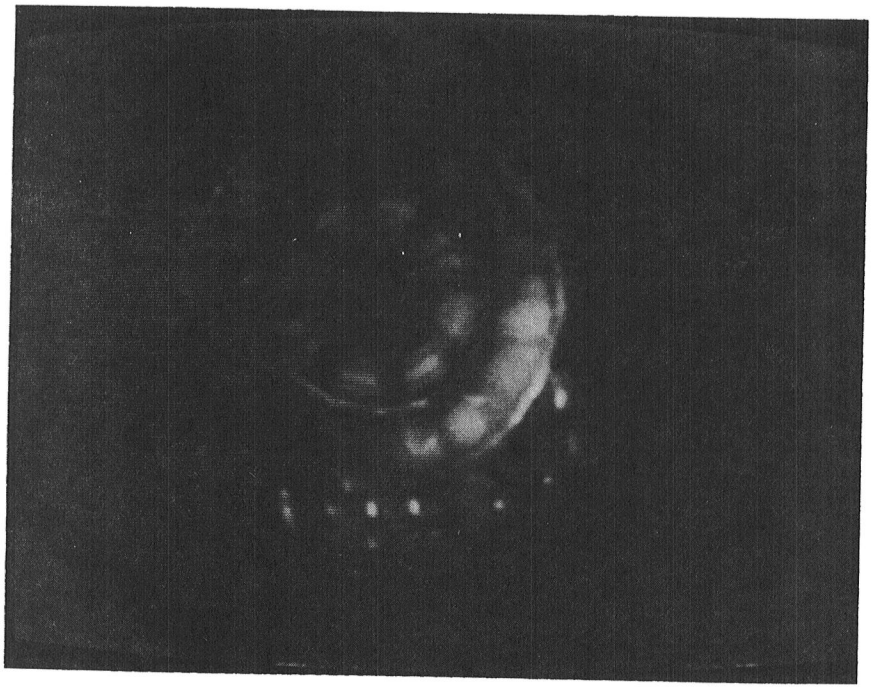

Figure 20. - Upstream view of engine at intermediate throttle position during stall.

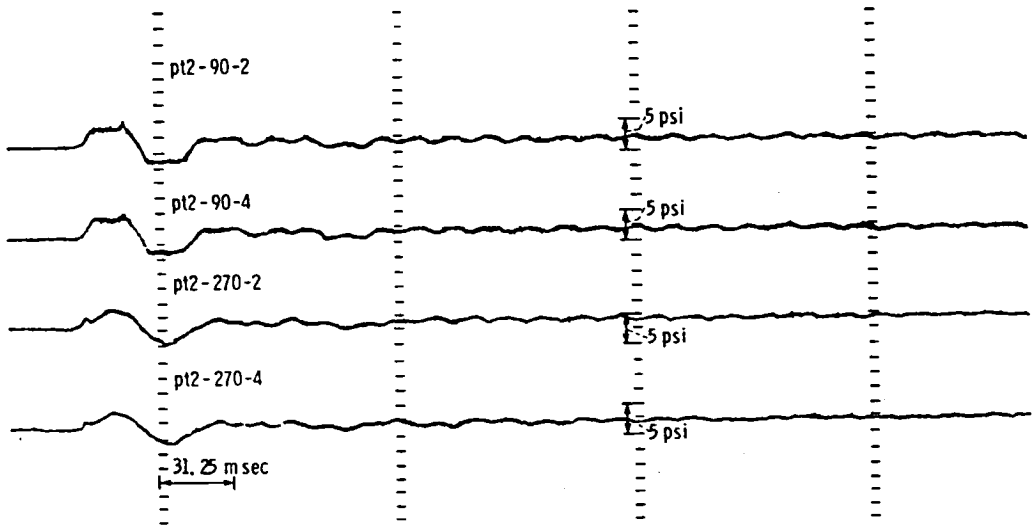

Figure 21. - Analog traces of engine inlet total pressure during the non-recoverable stall transient.

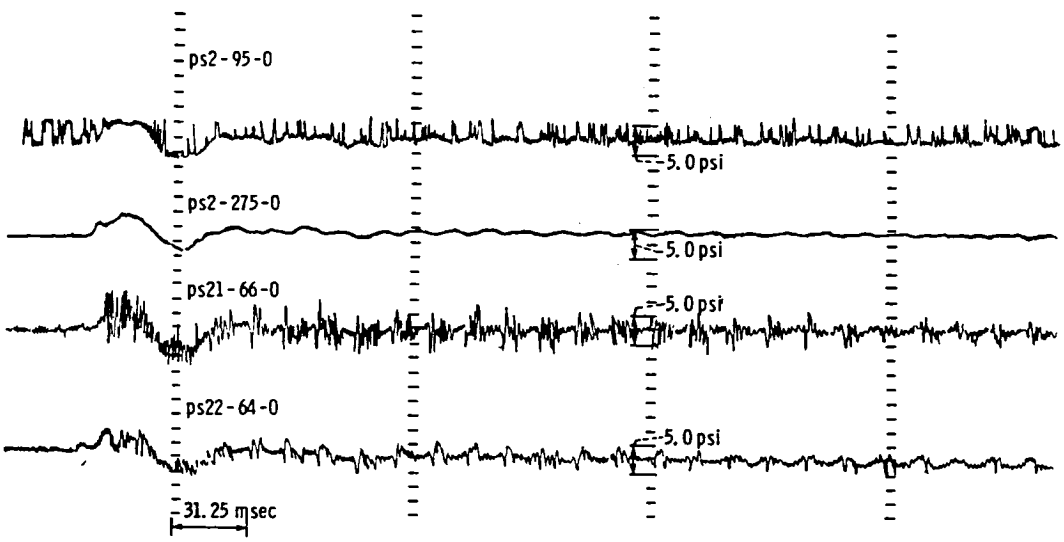

Figure 22. - Analog traces of fan inlet, and fan 1st and 2nd stage outer wall static pressures during the non-recoverable stall.

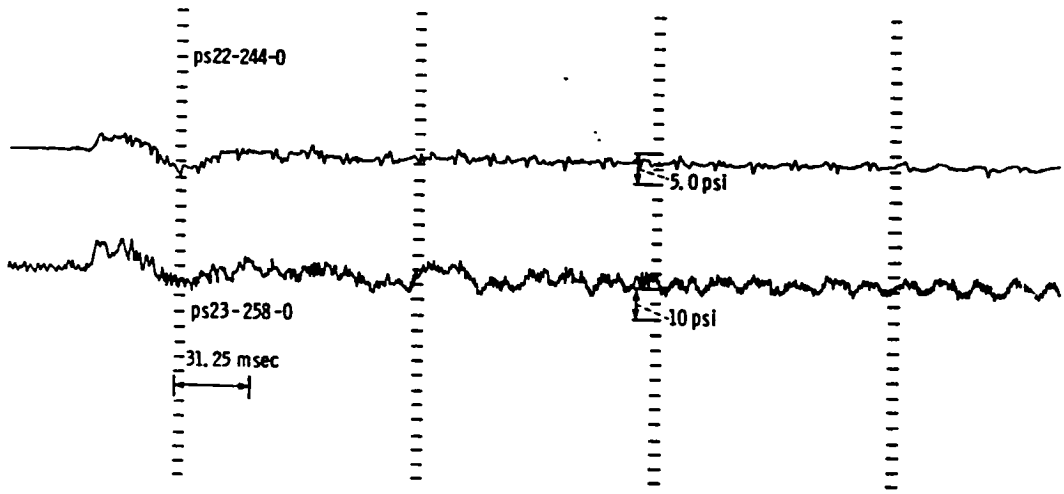

Figure 23. - Analog traces of fan 2nd and 3rd stage outer wall static pressures during the non-recoverable stall.

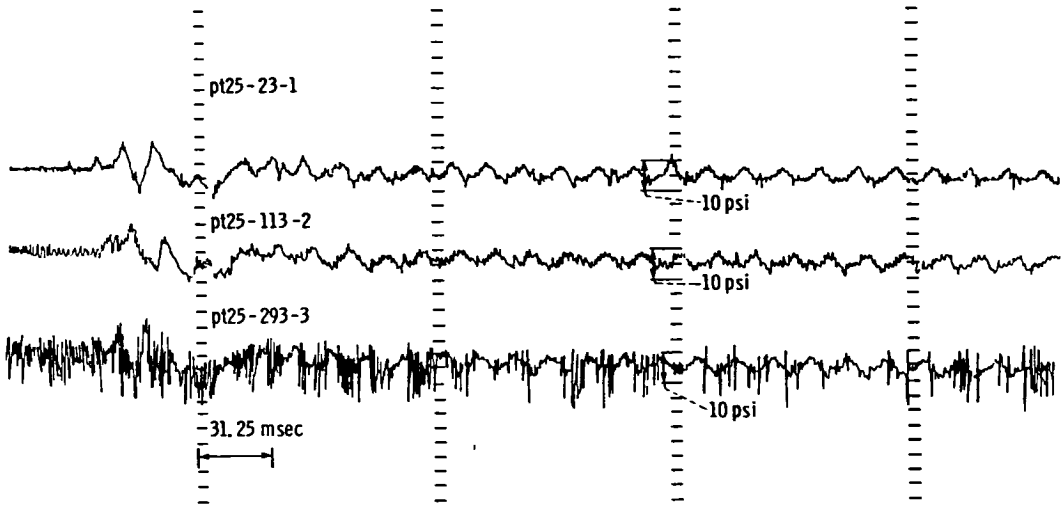

Figure 24. - Analog traces of core compressor inlet total pressure during the non-recoverable stall.

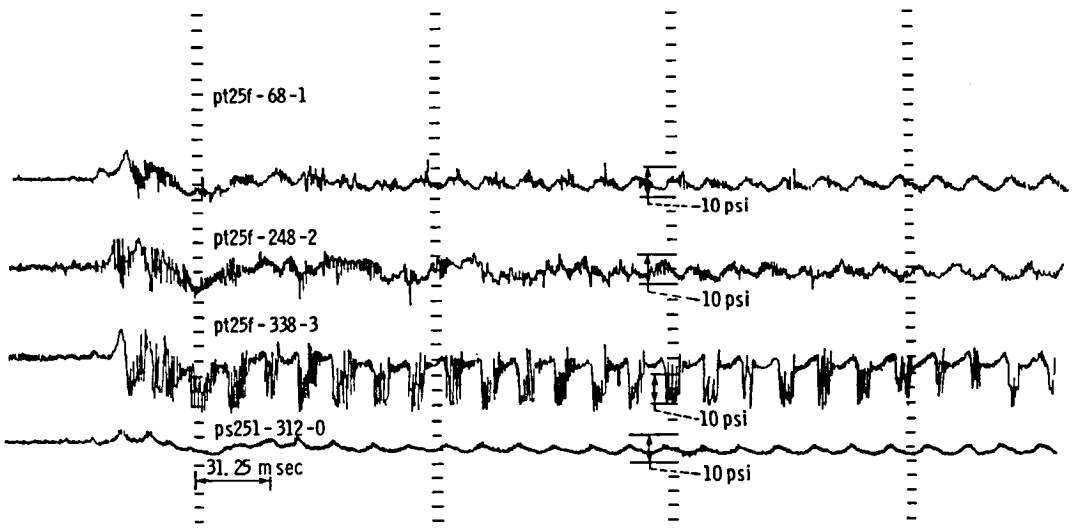

Figure 25. - Analog traces of fan duct inlet total pressure and 1st stage of core compressor static pressure during the non-recoverable stall.

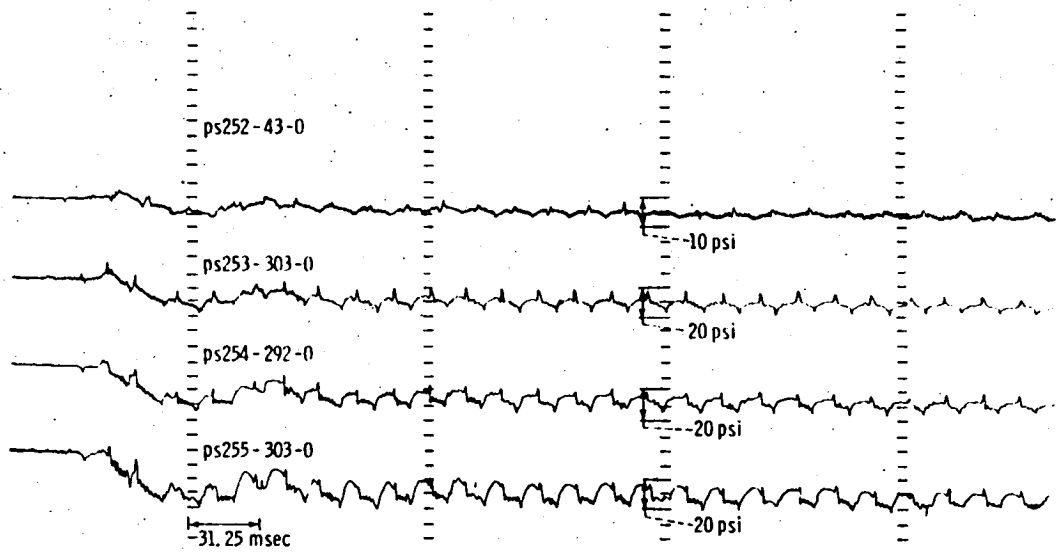

Figure 26. - Analog traces of core compressor stages 2 to 5 outer wall static pressures during the non-recoverable stall.

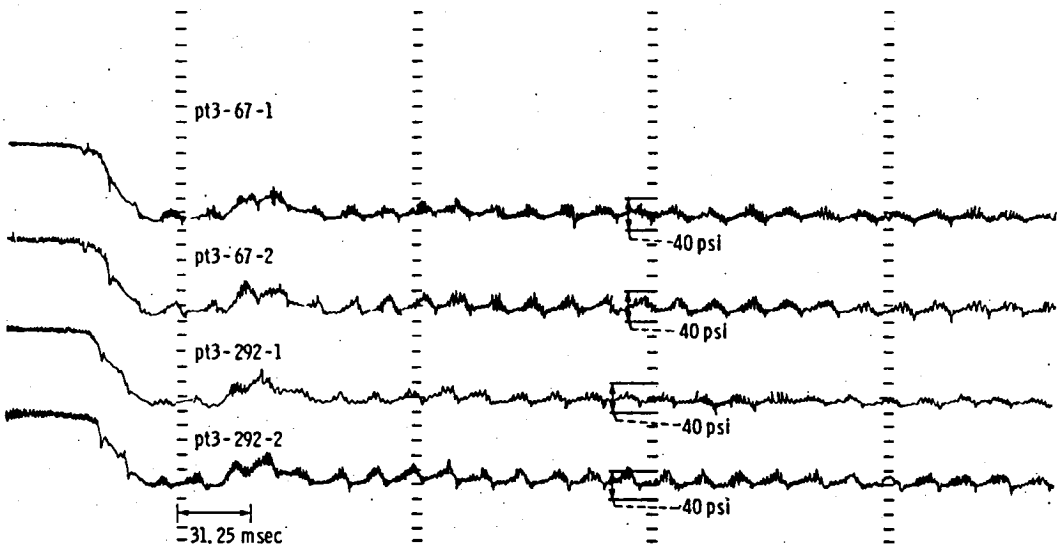

Figure 27. - Analog traces of core compressor exit total pressure during the non-recoverable stall.

1. Report No.	2. Government Accession No.	3. Recipient's Catalog No.
NASA TM-81759		

4. Title and Subtitle	5. Report Date
HIGH-RESPONSE MEASUREMENTS OF A TURBOFAN ENGINE DURING NONRECOVERABLE STALL	April 1981
	6. Performing Organization Code 505-32-6A
7. Author(s) Doug Lee	8. Performing Organization Report No. E-822
	10. Work Unit No.
9. Performing Organization Name and Address National Aeronautics and Space Administration Lewis Research Center Cleveland, Ohio 44135	11. Contract or Grant No.
	13. Type of Report and Period Covered Technical Memorandum
12. Sponsoring Agency Name and Address National Aeronautics and Space Administration Washington, D.C. 20546	14. Sponsoring Agency Code

15. Supplementary Notes

16. Abstract

This report presents high-response data recorded when a turbofan engine encountered nonrecoverable stall. High-response measurements of a Pratt and Whitney F100(3) turbofan engine at a simulated Mach number and altitude of 1.2 and 3000 m (10 000 ft) respectively were recorded during a nonrecoverable stall. The nonrecoverable stall occurred as a result of incorrect scheduling of the high-compressor variable vanes (RCVV) during an experimental engine control investigation. Off-schedule RCVV was caused by a time lag in the RCVV switching mechanism during engine deceleration. Recorded data indicates rotating stall originating in the high-pressure compressor. From this region the disturbance propagates upstream into the fan and downstream throughout the core compressor. Core compressor rotational speed had decreased, as a result of throttle movement, from 12 790 rpm to 10 800 rpm at the onset of stall. Rotating stall developed in the fan and high-pressure compressor at a frequency of 66 hertz. The rotating stall remained in the core compressor until the engine was shutdown. The fan exhibited some rotating stall, but the amplitude of the pressure oscillations were less severe. Data indicates that the fan was able to recover from the stall. Fan turbine inlet temperature (FTIT) had been decreasing until stall developed in the high-pressure compressor. From this time, FTIT increased towards its maximum temperature limit. Increasing FTIT occurring with decreasing core compressor rotational speed is a trend exhibited by other F100 engines during nonrecoverable stall. The rising FTIT during nonrecoverable stall may be the result of incomplete combustion in the combustor and additional combustion occurring through the turbine.

17. Key Words (Suggested by Author(s))	18. Distribution Statement
Gas turbines; Stall; Turbofan; Nonrecoverable stall; Stagnation stall; Hung stall; Turbofan performance; Aircraft propulsion; Airbreathing engines	Unclassified - unlimited STAR Category 07

19. Security Classif. (of this report)	20. Security Classif. (of this page)	21. No. of Pages	22. Price*
Unclassified	Unclassified		

* For sale by the National Technical Information Service, Springfield, Virginia 22161

National Aeronautics and
Space Administration

Washington, D.C.
20546

Official Business
Penalty for Private Use, $300

SPECIAL FOURTH CLASS MAIL
BOOK

Postage and Fees Paid
National Aeronautics and
Space Administration
NASA-451

NASA

POSTMASTER: If Undeliverable (Section 158
Postal Manual) Do Not Return